

Modeling the dynamics of metabolism in montane streams using continuous dissolved oxygen measurements

Christian Birkel,¹ Chris Soulsby,¹ Iain Malcolm,² and Doerthe Tetzlaff¹

Received 18 September 2012; revised 7 July 2013; accepted 8 July 2013.

[1] We inferred in-stream ecosystem processes in terms of photosynthetic productivity (P), system respiration (R), and reaeration capacity (RC) from a five parameter numerical oxygen mass balance model driven by radiation, stream and air temperature, and stream depth. This was calibrated to high-resolution (15 min), long-term (2.5 years) dissolved oxygen (DO) time series for moorland and forest reaches of a third-order montane stream in Scotland. The model was multicriteria calibrated to continuous 24 h periods within the time series to identify behavioral simulations representative of ecosystem functioning. Results were evaluated using a seasonal regional sensitivity analysis and a colinearity index for parameter sensitivity. This showed that >95 % of the behavioral models for the moorland and forest sites were identifiable and able to infer in-stream processes from the DO time series for around 40% and 32% of the time period, respectively. Monthly P/R ratios <1 indicate a heterotrophic system with both sites exhibiting similar temporal patterns; with a maximum in February and a second peak during summer months. However, the estimated net ecosystem productivity suggests that the moorland reach without riparian tree cover is likely to be a much larger source of carbon to the atmosphere ($122 \text{ mmol C m}^{-2} \text{ d}^{-1}$) compared to the forested reach ($64 \text{ mmol C m}^{-2} \text{ d}^{-1}$). We conclude that such process-based oxygen mass balance models may be transferable tools for investigating other systems; specifically, well-oxygenated upland channels with high hydraulic roughness and lacking reaeration measurements.

Citation: Birkel, C., C. Soulsby, I. Malcolm, and D. Tetzlaff (2013) Modeling the dynamics of metabolism in montane streams using continuous dissolved oxygen measurements, *Water Resour. Res.*, 49, doi:10.1002/wrcr20409.

1. Introduction

[2] The metabolism of aquatic ecosystems is a first-order control on the carbon cycle of streams. Understanding of the factors which regulate the dynamics of in-stream metabolism is a prerequisite to assessing ecosystem function [Williamson *et al.*, 2008]. Most studies show that terrestrial freshwaters (lakes and rivers) are heterotrophic systems that act as sources of carbon to the atmosphere [Aufdenkampe *et al.*, 2011]. However, photosynthetic production and system respiration need to be quantitatively assessed to estimate the current metabolic characteristics of different types of streams and to project potential regional climate change implications and possible mitigation measures [Cole *et al.*, 2007]. In small steep headwater streams, the benthos—i.e. the community of organisms living in, on or near the streambed—has a much greater biomass than the water column and benthic photosynthesis and respiration

usually dominate in-stream metabolism. However, the spatial and temporal variations in these processes are usually poorly understood.

[3] Several methods have been developed to estimate in-stream metabolism using in situ measurement of dissolved oxygen (DO) changes (see Bott [2006] and review by Staehr *et al.* [2012]). In this study, we focus on mass balance modeling in conjunction with high-resolution, longer-term DO data as a basis for estimating community photosynthesis (P) and respiration (R) from simulation of diurnal DO dynamics. Since the first approach to determining stream metabolism proposed by Odum [1956] was published, technical progress in computing power and reliable continuous monitoring equipment (such as stable optic DO sensors) allows relatively simple numeric analysis of high-frequency, long-term data at multiple spatial scales [Malcolm *et al.*, 2006; Roberts *et al.*, 2007]. Numerical models that analyze continuous long-term DO data to assess ecosystem processes have recently become freely available, e.g., the EXCEL-based program RIVERMET by Izaguirre *et al.* [2007] and a similar model applied to the lagoon of Venice by Ciavatta *et al.* [2008]. Both approaches use the night-time regression method of Kelly *et al.* [1974] to estimate reaeration capacity (RC) and R from measured DO and then calibrate photosynthesis parameters to estimate P. The latter method has the advantage of reducing the number of model parameters which are directly derived from measured data and hence also

¹School of Geosciences, Northern Rivers Institute, University of Aberdeen, Aberdeen, Scotland, UK.

²Marine Science Scotland, Freshwater Laboratory, Pitlochry, Scotland, UK.

Corresponding author: C. Birkel, School of Geosciences, Northern Rivers Institute, University of Aberdeen, Aberdeen AB23 4UF, Scotland, UK. (c.birkel@abdn.ac.uk)

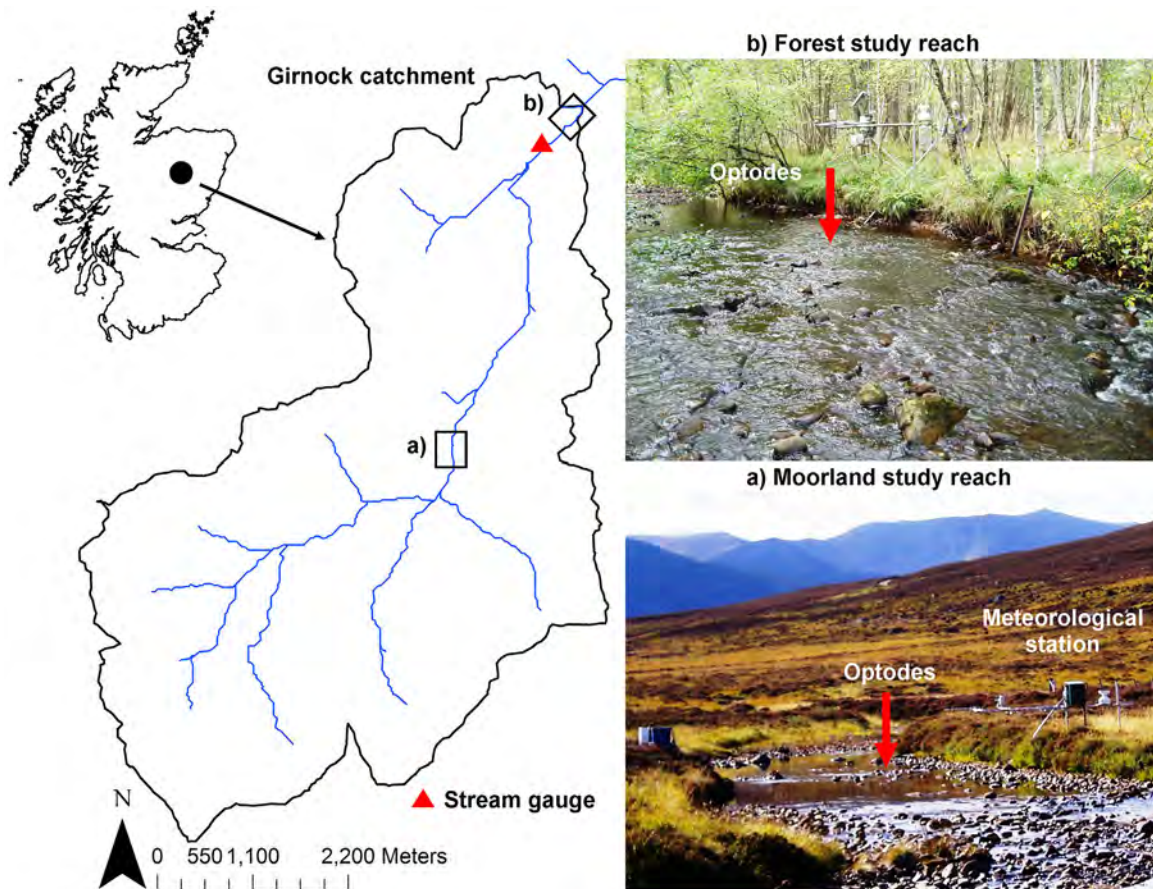


Figure 1. (a) The moorland and (b) the forest study reaches under summer low flow conditions with approximate equipment location indicating the main difference in riparian vegetation in the upland Girnock catchment in Scotland.

reducing the associated uncertainty. However, the approach needs further testing in upland rivers.

[4] Common and often serious limitations of modeling approaches using inverse calibration of model parameters to fit observed data are the selection of appropriate model structures and the identifiability of model parameters both of which can lead to the propagation of uncertainty [Beven, 2012]. Even though numerical oxygen mass balance models are less sensitive to measurement noise and are less constrained by the exacting assumptions often needed with analytical approaches [e.g., Kelly et al., 1974; Valino et al., 2005], models that are too simple may not adequately represent the dominant processes influencing metabolism dynamics. In contrast, overparameterized models may lead to errors in predictions and results that are equifinal [Beven, 2012]. This has been shown for oxygen mass balance models, where increasing complexity at the expense of increased parameterization (e.g., in the case of incorporation of a nonlinear light saturation productivity term) did not necessarily lead to improved performance over linear light-productivity formulations [Hanson et al., 2008]. These problems can be partly addressed using a flexible, yet process-based modeling approach, where the model structure solely depends on the information content of the data. In terms of in-stream metabolism, empirical observations of sinusoidal or nonideal diurnal oxygen dynamics

can be used to evaluate model performance. Applications of simple mass balance models can thus be considered as “behavioral,” or a successful representation of the in-stream processes of photosynthesis and respiration, if diurnal oxygen dynamics can be simulated accurately. The challenge here is to select and retain behavioral models based on posterior analysis such as, parameter sensitivity analysis or direct scrutiny while calibrating the model [e.g., Hornberger and Spear, 1981]. Alternatively, Holtgrieve et al. [2010] presented a Bayesian approach of oxygen mass balance modeling with explicit uncertainty analysis. Therefore, any deviation from behavioral models may be taken as indicative of other processes affecting the oxygen balance. These might include hydrological influence such as flood events (which increase water depth and decrease clarity through associated increases in turbidity and dissolved organic carbon (DOC), thus decreasing radiation inputs to the stream bed), ground and soil water inflows, hyporheic exchange flows, radiation variability, and anthropogenic influence which may disturb the diurnal oxygen pattern and cause the model to fail [Demars et al., 2011a; Uehlinger et al., 2000]. There is also considerable uncertainty as to the seasonal and event-based changes in the benthic biomass, as well as the role of organisms in the hyporheic zone and how they influence stream metabolism reflected in DO curves [Marmonier et al., 2012].

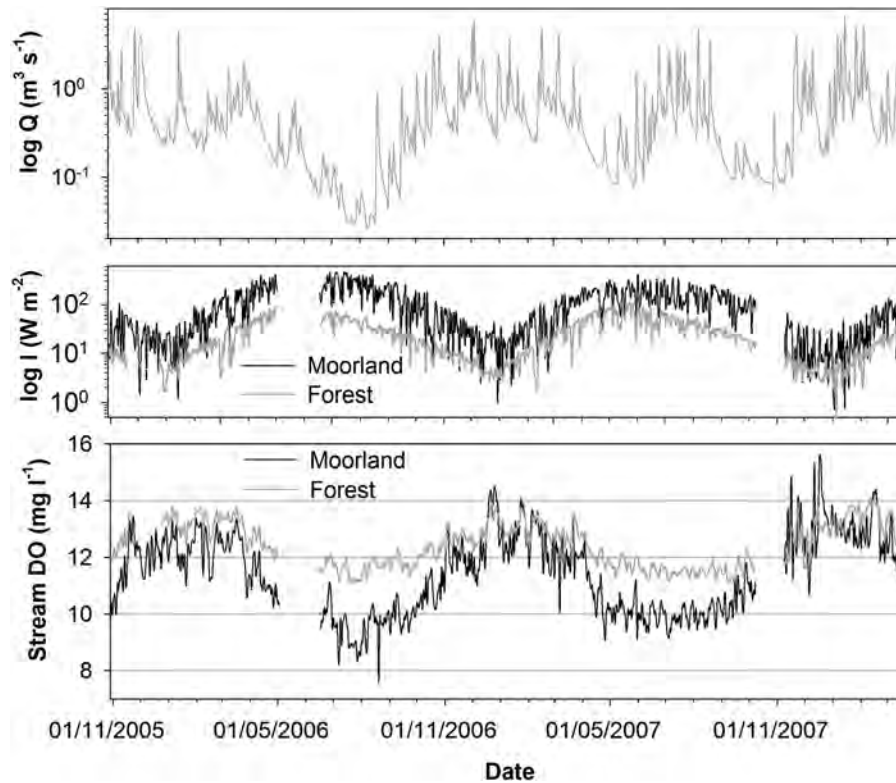


Figure 2. Mean daily hydrological (discharge Q , log scale), meteorological (incoming short-wave radiation I , log scale) and dissolved oxygen (DO) data for the moorland and forest reaches of the Girnock Burn. Note that the discharge data are given for the forest site only to improve visualization.

[5] In this article, we build on previous work from the intensively studied upland stream, the Girnock Burn, in the Cairngorm Mountains in Scotland. The Girnock has been the focus of population studies of Atlantic salmon (*Salmo salar*) since the mid-1960s, and recent interdisciplinary research has explored numerous aspects of the ecology, biogeochemistry, and hydrology of the stream [e.g., Moir *et al.*, 2002; Malcolm *et al.*, 2005; Tetzlaff *et al.*, 2007; Birkel *et al.*, 2011; Imholt *et al.*, 2012]. However, a major gap in the Girnock research is the lack of any assessment of in-stream metabolism. The upper catchment is unforested moorland, while in the lower catchment, the stream is fringed by broadleaved deciduous woodland. Previous work has shown that the riparian woodland has a marked effect on the stream energy balance and temperatures [Hannah *et al.*, 2008]. Given the dominance of incoming short-wave radiation and allochthonous inputs in driving photosynthesis, it is hypothesized that the forest and moorland reaches of the river will have very different metabolism dynamics. To this end, it provided an opportunity to develop an appropriate modeling approach that could estimate the key components of stream metabolism. The specific objectives of the study were:

[6] 1. To develop a parsimonious yet flexible and time-variable mass balance modeling approach to estimate stream metabolic process dynamics (P and R). This would use long-term, high-resolution simulation of DO measurements in two distinct reaches of an upland stream characterized by high channel roughness and no reaeration measurements available. Emphasis is put on the identifi-

ability of model parameters specifically for the case of simultaneous calibration of reaeration, P and R, and subsequent identification of behavioral simulations.

[7] 2. To assess the temporal (seasonal to annual) variability of controls on stream metabolism and the differences between forest and moorland reaches of the same river.

[8] 3. To explore influences—specifically riparian vegetation—on the simulated dynamics of community P and R by direct comparison of stream reaches.

2. Study Area and Data

[9] The physical characteristics of the Girnock catchment (Figure 1) are described in detail elsewhere [e.g., Tetzlaff *et al.*, 2007]. Briefly, the Girnock has many typical characteristics of catchments in the Scottish Highlands; it is dominated by heather moorland (*Calluna spp*) vegetation, granitic bedrock, and has wide valley bottom areas with typically saturated peaty soils, overlying low permeability glacial drift. In the lower catchment, riparian soils are more alluvial and support riparian forest dominated by Alder (*Alnus glutinosa*) [Malcolm *et al.*, 2008; Imholt *et al.*, 2012]. Average water balance components for the catchment approximate to 1000 mm/yr precipitation, 400 mm/yr evapotranspiration, and 600 mm/yr runoff. Discharge is measured by the Scottish Environment Protection Agency (SEPA) in a naturally rated section of the lower river (Figure 1). At this point, the Girnock is a third-order stream and exhibits a flashy hydrograph (see Figure 2) mainly due to near-surface runoff generation processes

Table 1. Stream Reach Characteristics and Summary Statistics of Environmental Variables at the Moorland and Forest Sites of the Girnock Experimental Catchment

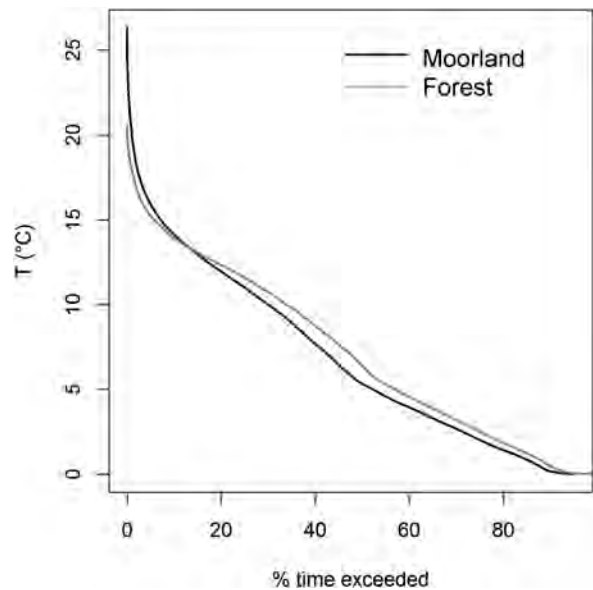
| | Variable | Unit | Min | Mean | Max | CV |
|----------|--|--------------------------------|-------|-------|-------|------|
| Moorland | Channel width (w) | m | / | 9 | / | / |
| | Elevation (E) | m.a.s.l. | / | 310 | / | / |
| | Discharge (Q) for catchment area of 25 km ² | m ³ s ⁻¹ | 0.026 | 0.57 | 20.9 | 1.56 |
| | Stream velocity (v) | m s ⁻¹ | 0.014 | 0.11 | 1.74 | 0.93 |
| | Stream depth (h) | m | 0.17 | 0.36 | 1.12 | 0.30 |
| | Dissolved oxygen (DO) | mg l ⁻¹ | 2.77 | 11.27 | 15.67 | 0.13 |
| | Stream temperature (T) | °C | 0 | 7.05 | 27.8 | 0.77 |
| | Radiation (I) | W m ⁻² | 0 | 111 | 1266 | 1.84 |
| Forest | Channel width (w) | m | / | 9 | / | / |
| | Elevation (E) | m.a.s.l. | / | 250 | / | / |
| | Discharge (Q) for catchment area of 31 km ² | m ³ s ⁻¹ | 0.026 | 0.62 | 20.9 | 1.57 |
| | Stream velocity (v) | m s ⁻¹ | 0.016 | 0.14 | 1.99 | 0.93 |
| | Stream depth (h) | m | 0.18 | 0.40 | 1.19 | 0.30 |
| | Dissolved oxygen (DO) | mg l ⁻¹ | 8.28 | 12.12 | 15.59 | 0.15 |
| | Stream temperature (T) | °C | 0 | 7.07 | 20.6 | 0.72 |
| | Radiation (I) | W m ⁻² | 0 | 25.7 | 510 | 1.84 |

quickly contributing water from the riparian saturation areas to the stream [Birkel *et al.*, 2010, 2011]. Due to the glacial history of the landscape, the river valley is relatively wide, shallow, and gently sloping (average gradient 0.0092 m m⁻¹). Given the geology and landuse, the Girnock is a nutrient-limited system: weekly sampling campaigns have revealed mean annual nitrate concentrations at 0.18 mg l⁻¹ and standard deviation of 0.1 mg l⁻¹ [Smart *et al.*, 2001]. Phosphate concentrations were always below detection limit throughout the sampling campaign. However, an autumn nitrate pulse and episodic flushing of organic soil material and feces [Tetzlaff *et al.*, 2010] from relatively high densities of grazing deer (21 animals per km² according to Thomson *et al.* [2006]) during storm events can enhance nutrient availability to ecosystem metabolism.

[10] The two stream reaches investigated have been intensively studied mainly in relation to fish population dynamics. Atlantic salmon spawning activities can occur in both reaches and stream, and hyporheic oxygen levels have been monitored to assess their influence on egg survival [e.g., Moir *et al.*, 2002; Malcolm *et al.*, 2005]. Both stream reaches are instrumented with meteorological stations (Campbell Scientific) observing air temperature (AT), humidity (H), incoming short-wave radiation (I), net radiation (NR), and precipitation for hydroclimate [Hannah *et al.*, 2008]. In addition, Aandera 3830 optodes have been installed to measure stream temperature (T) and DO at a 15 min time step (Figures 1 and 2). The optodes were calibrated in the laboratory and precisions determined at ± 0.1 °C and $\pm 1\%$ DO and then deployed on the streambed [Malcolm *et al.*, 2006].

[11] The main differences between the study reaches are dominated by the riparian vegetation cover for the open moorland site and a 2 km length of channel downstream which is under forest canopy (see photos in Figure 1, Table 1). The shading effect of the riparian forest is clearly evident in significantly reduced incoming short-wave radiation (Figure 2), which also exerts a cooling effect on stream temperatures specifically during summer (Figure 3). In-stream plant surveys showed extensive algae, biofilms, and macrophyte growth at both sites. However, the main macrophytes such as Bog Pondweed (*Potamogeton polygonifolius* Pourr.), Lesser Spearwort (*R. Flammula* L.),

Jointed Rush (*Juncus articulatus* L.), and Floating Sweet Grass (*Glyceria fluitans* L.) were only found at the moorland reach during summer. The shading of riparian forest cover seems to prevent macrophyte growth during summer, which was only observed at the forest reach early in spring (February/March) before leave development. Hydraulic conductivities of the coarse-grained gravel ($D_{50} = 43.4$ mm) streambed sediment (low fine sediment content, <12%) forming the hyporheic zones of both reaches were estimated to range between 1×10^{-5} and 6×10^{-4} m s⁻¹ typically decreasing with depth [Malcolm *et al.*, 2011]. The coarse nature of the stream bed ensure that hydraulic roughness is high and turbulence is high in local steep sections facilitating reaeration at all flows. Additionally, there is a weir at a fish trap, which has a hydraulic drop of around 2 m and is located about 300 m upstream from the forest measurement site.


Figure 3. Stream temperature percentage time exceedance curves for the moorland and forest study reaches, respectively.

3. Modeling Approach

[12] We used a numerical oxygen mass balance model to simultaneously infer in-stream metabolic processes (P, R) and RC by calibrating to the measured diurnal DO curves captured by the high-resolution, long-term data [Ciavatta *et al.*, 2008; Holtgrieve *et al.*, 2010]:

$$\frac{\partial DO}{\partial t} = \frac{RC + P - R}{h} \quad (1)$$

[13] The model uses air temperature time series ($^{\circ}\text{C}$), stream temperature time series ($^{\circ}\text{C}$), incoming short-wave radiation time series (W m^{-2}), sea level air pressure (P_{msl}) time series (kPa), and mean stream depth (h in m) as input data. The modeling procedure is relatively simple, yet consistent with the data available and can be summarized by the following steps. We explain data preprocessing and postprocessing as well as the model component functions (P, R, and RC) substituted into equation (1) to estimate whole-stream metabolism.

3.1. Data Preprocessing

[14] 1. To ensure adequate data quality control, all time series were visually screened to detect outliers, identify periods of potential sensor drift, and establish the occurrence of data gaps (missing values lead to removal of complete 24 h periods).

[15] 2. The hydraulic relationships for each study site were also established as part of the preprocessing using a discharge rating-curve (least-squares best-fit for $a = 0.22$ and $b = 0.72$) derived from manual flow gauging ($n = 89$). This related cross-sectional width (w in m), channel flow velocity (v in m s^{-1}), and depth (h) to discharge (Q in $\text{m}^3 \text{s}^{-1}$):

$$v_n = aQ^b \quad (2)$$

$$h = \frac{Q}{(vw)} \quad (3)$$

[16] 3. DO time series were also preprocessed: this involved the conversion (equation (4)) of measured dissolved oxygen saturation in % (O_{sat}) into concentrations (DO_{obs} in mg l^{-1}) via the expected oxygen solubility O_s based on air (AT) and stream (T) temperature and altitudinal-adjusted air pressure (P_E) similar to the procedure described by Demars *et al.*, [2011a]:

$$DO_{\text{obs}} = \frac{(O_{\text{sat}} O_s)}{100} \quad (4)$$

$$O_s = \frac{O_s^{\text{atm}} (P_E - V)}{(101.325 - V)} \quad (5)$$

where O_s is the expected oxygen solubility (mg l^{-1}), V is the saturation water vapor pressure (kPa), O_s^{atm} the oxygen solubility under normal pressure (mg l^{-1}), and P_E the altitudinally corrected pressure (kPa).

$$P_E = P_{\text{msl}} e^{-\left(\frac{mgE}{kAT}\right)}, \quad (6)$$

where P_{msl} is the pressure at mean sea level (kPa), $g = 9.806$ (m s^{-2}), m is the molecular mass of dry

air (kg mol^{-1}), and k is the Boltzmann constant (J K^{-1}).

$$V = 0.00005AT^3 + 0.001AT^2 + 0.0473AT + 0.6089 \quad (7)$$

$$O_s^{\text{atm}} = -0.00008T^3 + 0.008T^2 - 0.404T + 14.609 \quad (8)$$

[17] The 15 min raw data were then aggregated to hourly time steps to smooth out short-term measurement noise.

3.2. Model Component Functions

[18] Relevant in-stream ecosystem metabolic processes were conceptualized in the oxygen mass balance model of equation (1) as follows:

[19] 1. RC—The RC term refers to the net flux of oxygen across the water/atmosphere boundary. Due to the lack of direct oxygen solubility measurements (undertaking tracer gas experiments at different flow conditions were constrained by the remoteness of the site and health and safety issues) and the uncertainties surrounding empirical reaeration equations [e.g., Genereux and Hemond, 1992], we adopted the reaeration coefficient k_a (h^{-1}) as a calibrated model parameter depending on the oxygen deficit $D = DO_{\text{sat}} - DO_{\text{obs}}$ per hourly time step (similar to Holtgrieve *et al.* [2010]). The sign of D (positive = oxygen deficit, negative = oxygen super-saturation) usually indicates the direction of oxygen flux from or to the atmosphere. However, we allowed negative k_a values for calibration (Table 2). First, we allowed this as a test for the model to consistently select the most plausible parameter combination in terms of ecosystem processes. Second, negative k_a values could represent frequently observed diurnal oxygen curves during times (winter) the stream was super-saturated with oxygen as a result of the weir creating high turbulence upstream of the Forest site. The reaeration model function RC for use in the mass balance model of equation (1) is given here:

$$RC = k_a T(D) \quad (9)$$

with

$$k_a T = k_a \theta^{T-20} \quad (10)$$

where θ was set to 1.0241 [Elmore and West, 1961].

[20] 2. Respiration (R)—The temperature corrected community respiration for the in-stream ecosystem is estimated using equation (11) originally proposed by Parkhurst and Gulliver [1998]:

$$R = (R_{20} + \beta I) \theta^{T-20} \quad (11)$$

[21] This nonlinear function accounts for photo-respiration during the day-time (parameter β relates the amount of light received to the respiration rate) as well as night-time respiration (standard total dark community respiration rate parameter R_{20} at 20 $^{\circ}\text{C}$). The effect of photo-respiration and varying stream depth (equation (11) substituted into equation (1)) on ecosystem respiration (ER) is shown in Figure 4 (increasing photo-respiration increases respiration rates at constant depths, but with greater stream depth the activation threshold of respiration also increases). Setting β to 0 implies no photo-respiration (the term βI is

Table 2. Model Performance (SSE), Initial Parameter Ranges Used for Optimization and Overall 10th and 90th Percentiles of Posterior Parameter Ranges for the Moorland and the Forest Site (in Italics)

| Parameters | Units | Initial Parameter Ranges | Posterior 10th and 90th Parameter Percentiles |
|---------------------------|--|--------------------------|--|
| k_a | h^{-1} | $[-10, 10]$ | $[0.01, 0.90]$ <i>$[-0.52, 0.79]$</i> |
| R_{20} | $\text{mg O}_2 \text{ l}^{-1} \text{ h}^{-1}$ | $[0, 2]$ | $[4 \times 10^{-8}, 0.71]$ <i>$[1.4 \times 10^{-14}, 0.19]$</i> |
| β | $\text{mg O}_2 \text{ W}^{-1} \text{ h}^{-1}$ | $[0, 1]$ | $[1.9 \times 10^{-6}, 0.007]$ <i>$[1.2 \times 10^{-4}, 0.025]$</i> |
| p_1 | $(\text{mg O}_2 \text{ W}^{-1} \text{ h}^{-1})^{-1}$ | $[0, 5000]$ | $[2.2 \times 10^{-4}, 1973]$ <i>$[1.4 \times 10^{-3}, 943]$</i> |
| p_2 | $(\text{mg O}_2 \text{ l}^{-1} \text{ h}^{-1})^{-1}$ | $[0, 50]$ | $[0.04, 31.5]$ <i>$[0.0015, 28.8]$</i> |
| SSE | mg l^{-1} | | $[0.04, 0.41]$ <i>$[0.05, 0.84]$</i> |
| Number of accepted models | 24 h periods | 769 760 | 305 (40%) 243 (32%) |

dropped) and equation (11) defaults to only one parameter (R_{20}).

[22] 3. Photosynthetic production (P)—was conceptualized in a similar way to *Uehlinger et al.* [2000] allowing for a switch between a linear (parameter p_1) and nonlinear light-saturation (parameter p_2) radiation-production relationship (equation (12) for use in equation (1)):

$$P = \frac{I}{p_1 + p_2 I} \quad (12)$$

[23] Figure 4 demonstrates radiation-production relationships for different parameterizations and the influence of stream depth. P decreases with increasing stream depth due

to decreased light penetration. If p_2 becomes zero, equation (12) defaults to only one parameter (p_1) similar to equation (11) simulating R (term $p_2 I$ is dropped). This might be viable in an energy-limited environment like Scotland where light saturation (represented by p_2) is potentially unlikely to be reached.

[24] Equation (1) is numerically solved for hourly time steps using a fourth-order Runge-Kutta integration scheme for numerical stability. The first observed oxygen concentration value at time 00:00 was assigned as starting value and excluded from evaluation. The mass balance C code was implemented into a script using the open source R language [R Core Development Team, 2010]. The integration of simulated j hourly P, R, and RC rates results in daily

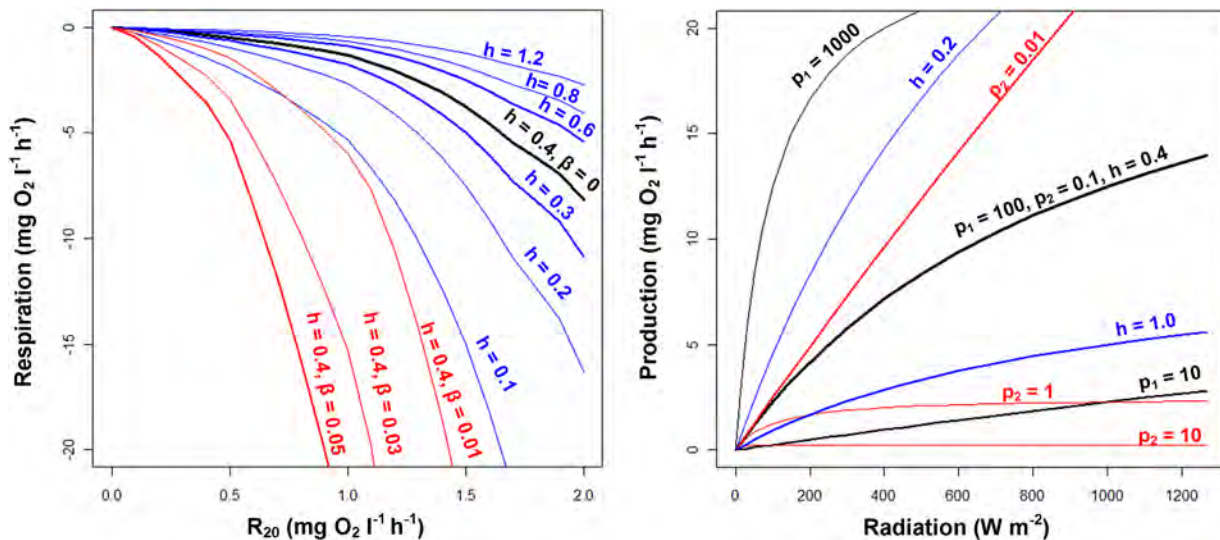


Figure 4. Simulated respiration response from equation (11) across the whole range of the respiration rate parameter R_{20} and observed temperatures is shown. The dependence of respiration activity to stream depth (h in meters) and influence of photo-respiration as indicated by parameter β are also shown. Please, note the negative sign for the respiration process visualizing oxygen consumption as opposed to oxygen production. The production-radiation relationship simulated with equation (12) is given for different parameter values showing effects of potential light saturation (for large p_2 and p_1), linear dependence (for small p_2 in red) and photo-inhibition due to increasing stream depth (h in meters) for constant p_2 and p_1 . Blue color reflects varying stream depth and red color variable light-respiration and productivity parameter p_2 .

photosynthetic production (GPP), daily ER, and daily reaeration (RC) similar to equation (13):

$$\text{GPP} = \int_j P dt \quad (13)$$

3.3. Model Calibration

[25] A total number of five model parameters (k_a , β , R_{20} , p_1 , p_2) were then iteratively calibrated to single 24 h periods by running through the complete DO time series using the associated climate variables to drive the model. The parameters are assumed to be constant over 24 h, but are allowed to vary between days and seasons in an attempt to assess parameter variations driven by climatic variability as well as unknown biological shifts in the systems behavior (e.g., caused by different seasonality in the growth periods of the benthic community and species scour induced by high flow conditions). Model structures are variable from a minimum of three (k_a , R_{20} , p_1) to the maximum five parameter model. Such a flexible model structure allows representation of processes which may be time variable—specifically light-saturation and photo-respiration—similar to *Parkhill and Gulliver* [1998] (see section 3.2 for explanation when parameters are dropped). Final model structure and parameter selection are determined by the relatively novel differential evolution (DE) optimization algorithm set to minimize the sum of squared errors (SSE) as an objective function [Mullen *et al.*, 2011]:

$$\text{SSE} = \sum_i^n (DO_{\text{sim}}^i - DO_{\text{obs}}^i)^2 \quad (14)$$

where the j simulated DO concentrations (DO_{sim}) minus the j observed DO concentration (DO_{obs}) represents the model residuals or error term.

[26] The DE algorithm has been shown to be particularly effective for the calibration of high-dimensional solution spaces which commonly characterizes even more highly parameterized environmental models [Andrews *et al.*, 2011]. The fundamental idea of evolutionary algorithms is based on natural selection where parameter populations are modified over following generations using arithmetic operations to minimize an objective function [Price *et al.*, 2006]. During this process, we retained the best parameter populations after every 50 evaluations until convergence toward a global minimum for the posterior parameter sensitivity analysis. Convergence properties in terms of performance were a priori assessed by repeated application of the DE optimization to selected days.

[27] It is clear that a single optimal parameter set is unlikely to be found in the presence of equifinal environmental models of complex aquatic systems [Beven, 2012]. However, as Andrews *et al.* [2011] demonstrated, most sophisticated optimization algorithms provide a solution representative of a near-optimal parameter set within the defined parameter space. Therefore, we report the residual error as likely parameter uncertainty in the form of simulation bounds after rejecting optimized models which are characterized by nonideal diurnal oxygen dynamics and are thus assumed to be nonrepresentative. By “non-ideal,” we

refer to oxygen dynamics that significantly deviate from a sinusoidal pattern due to processes not captured by the simple mass balance model (e.g., low-DO surface or groundwater influence during storm events). Optimized daily parameter sets were accepted as behavioral and assumed representative of the stream metabolism when

[28] 1. the calibrated objective function in form of the SSE (equation (14)) exceeds the 90th percentile of all 24 h period simulations and

[29] 2. simulated mean daily DO deviates by less than the 10th percentile of all simulations from the observed mean daily DO value.

[30] Both criteria are assumed to reflect (1) evaluation of the form of the diurnal oxygen pattern around (2) a center value (mean) of oxygen concentration.

3.4. Sensitivity Analysis

[31] A regional sensitivity analysis (RSA) was performed [cf. Hornberger and Spear, 1981] to assess whether model parameters exhibit the variability of productivity and respiration which might be reasonably anticipated. This included, for example capturing the general increase in productivity during the summer compared with winter. Therefore, all accepted (behavioral) daily model parameters were separated into autumn/winter (1 October to 31 March) and spring/summer (1 April to 30 September) periods and cumulated over the range of normalized model performance criteria as assessed by the sum of squared residuals (SSE). Curvature and constrained ranges indicate increased parameter identifiability across seasons (i.e., a straight diagonal line across the whole parameter range on the cumulative efficiency plot signals no seasonality of behavioral parameters).

[32] Furthermore, to ensure that the calibrated parameters for each 24 h period are identifiable, a colinearity index was calculated using all retained parameter populations during calibration (see also section 3.3). This colinearity index quantifies the linear dependence of parameters according to Brun *et al.* [2001]:

$$\gamma = \frac{1}{\sqrt{\min(EV[\hat{S}^T \hat{S}])}} \quad (15)$$

[33] The colinearity index γ is based on the eigenvalues EV of the sensitivity matrix S :

$$S_{i,j} = \frac{\partial y_i}{\partial \Theta_j} \frac{\Delta \Theta_j}{\Delta y_i} \quad (16)$$

where the i , j -th element of the normalized sensitivities in the sensitivity matrix S contains an output variable y_i at a certain time calculated by a model parameter Θ_j . The delta Δ indicates scaling of both components.

[34] The higher the value of γ , the more dependent are parameters. Dependent parameters could potentially generate similar output variables and are therefore not uniquely identifiable and cannot be determined by calibration. Parameter sets are considered independent and thus identifiable for a colinearity index of one (orthogonal) and reach infinity in the case of high dependency. Soetaert and

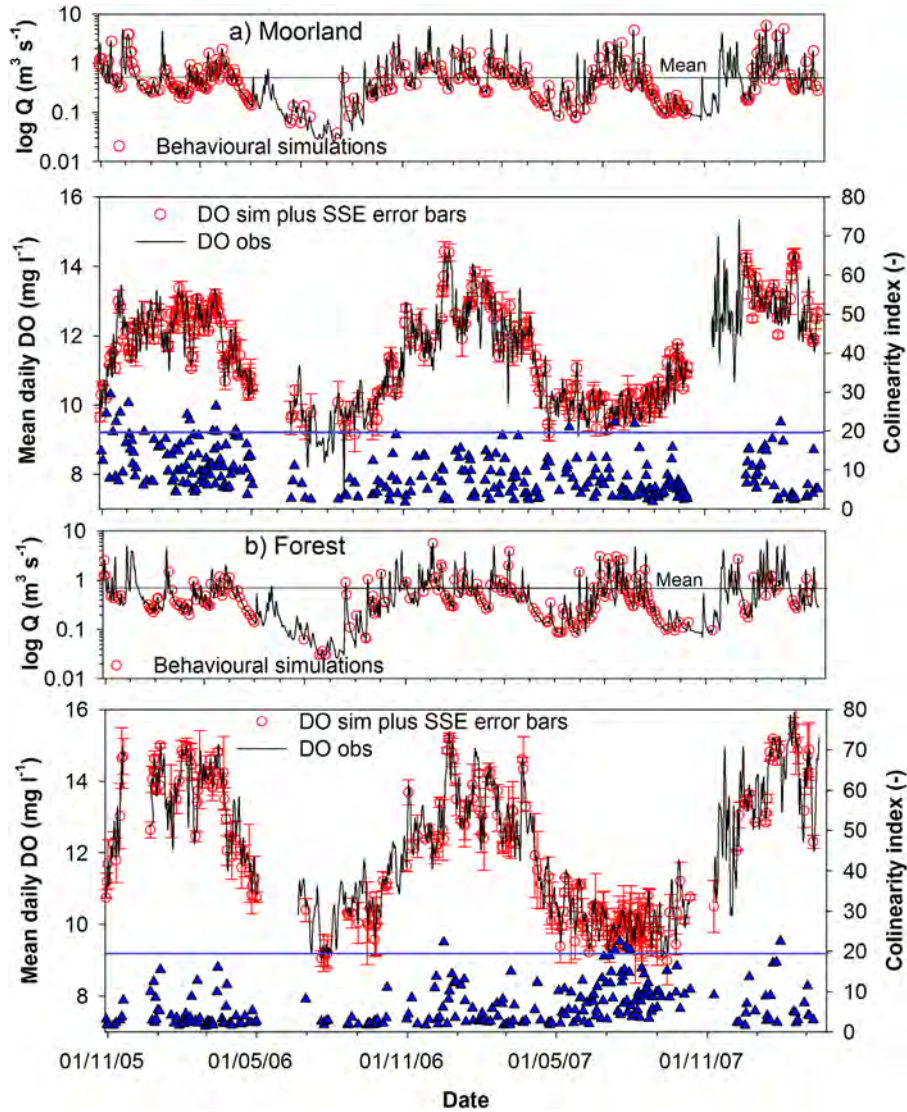


Figure 5. Behavioral daily DO model simulations (minimized sum of squared residuals, mean absolute error, and physically meaningful photosynthesis parameter) for the (a) moorland and (b) forest reaches of the Girnock Burn, respectively, indicating flow conditions. Error bars reflect the sum of squared residuals and the black lines indicate the mean discharge. The blue triangles show calculated collinearity indices around a critical threshold of 20 (blue line).

Petzold [2010] suggest a threshold value of $\gamma < 20$ to detect practical parameter identifiability.

4. Results

4.1. Environmental Characteristics Influencing DO Concentrations

[35] Figure 2 shows the time series between October 2005 and March 2008 for the main variables used to aid the modeling process. Hydroclimatic conditions were varied and as a result stream flows captured much of the range of seasonal and interannual variability that the catchment experiences. Precipitation shows limited seasonality in this part of Scotland and storm events can occur throughout the year, though westerly frontal systems typically cause higher flow conditions during the winter. Overall, the 2005/06 hydrological year (October to September) was charac-

terized by drier than average conditions and a marked summer low flow period. In contrast, 2006/07 was wetter than average, with an unusually wet summer.

[36] Incoming short-wave radiation (I) shows a seasonal summer (high radiation) and winter (low radiation) pattern at both sites. However, the riparian tree cover at the downstream forested site results in significantly less radiation reaching the stream (Table 1). The seasonal stream temperature pattern at both sites tracks that of the incoming short-wave radiation with the forest site exhibiting a cooling effect during summer and warming of the stream in winter [Malcolm *et al.*, 2008]. Note that the winter of 2005/06 was much cooler compared to 2006/07 at both sites. The stream temperature differences evident in Figure 3 are also to an extent reflected in the different DO patterns (see Figure 2) with the forest site exhibiting higher concentrations in winter and summer, but less seasonal amplitude compared to

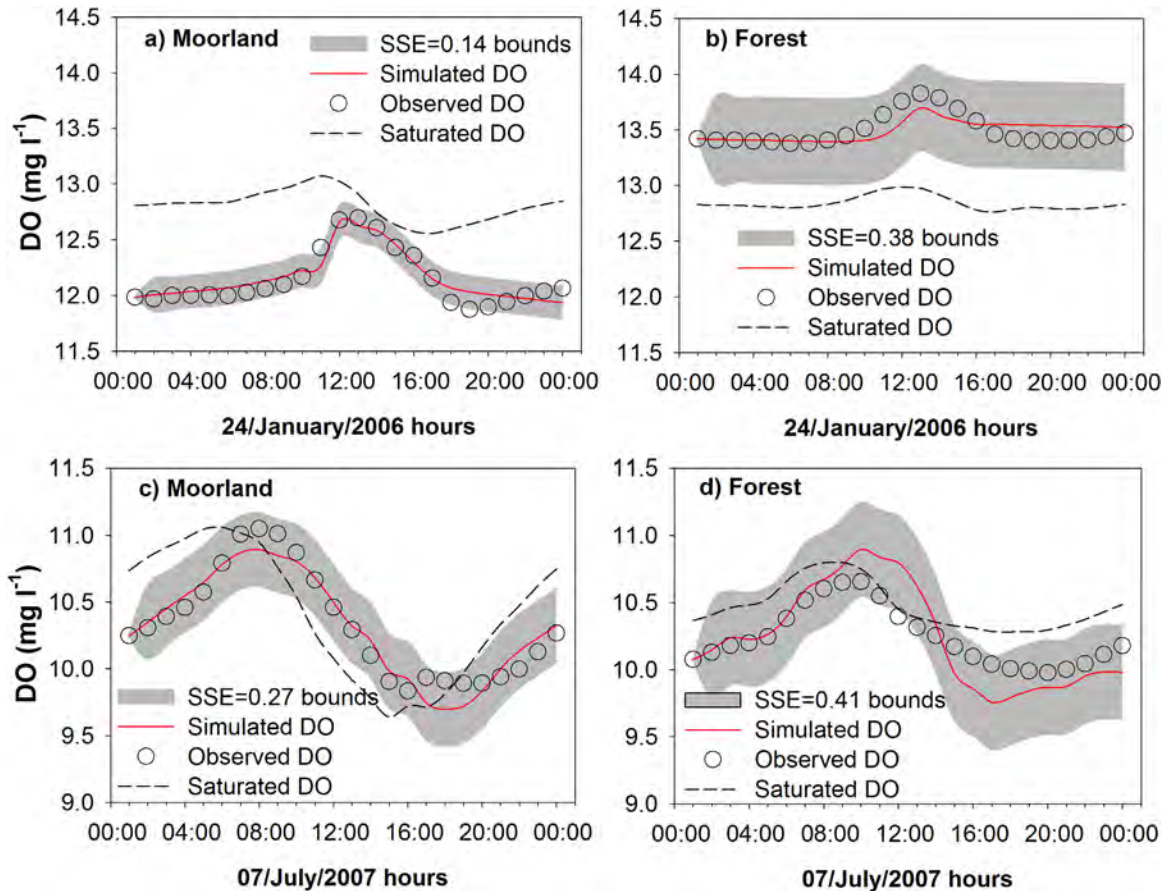


Figure 6. Simulated hourly DO at the moorland and forest sites for a selected winter (24 January 2006) and summer (7 July 2007) 24 h period. Uncertainty is given as simulation bounds reflecting the sum of squared errors (SSE) for the respective periods and sites as well as the saturated DO. The winter period was selected demonstrating typical differences between sites in terms of the frequently observed oxygen super-saturation at the forest site compared to the moorland. The summer period was chosen as an example for an unusual observed DO peak in the morning hours rather than mid-day coinciding with an incoming radiation peak and subsequent cloud cover.

the moorland site. The DO concentrations were similar at both sites only for the coldest winter temperatures. The moorland site is characterized by lower minimum DO concentrations in summer (e.g. August 2006) which are not experienced at the forest reach. In addition to the seasonal pattern, radiation, temperature, and DO exhibit marked diurnal variability which is not visible in the time series plots from Figure 2 which shows daily means.

4.2. Inferring Stream Metabolism From Continuous DO Measurements

[37] We applied the numerical oxygen mass balance model to the continuous DO data at both reaches. The model was fitted separately to 769 and 760 24-h periods for the moorland and forest site, respectively. This resulted in an optimized parameter set for every day of the 2005/08 study period. However, the models accepted as behavioral (e.g., the minimized SSE and deviations from the mean daily DO concentrations exceeded and were below the 90th and 10th percentile, respectively) account for around 40% (305) and 32% (243) of the total parameters sets derived for the study period for the moorland and forest site

(Figure 5). Accepted simulations are equally able to capture the distinct summer and winter seasonal DO dynamics at both sites. Parameter sensitivity analysis showed that >95% of accepted simulations are below a critical threshold of the colinearity index $\gamma = 20$ (Figure 5). This suggests that most parameters are identifiable in case of acceptable model performance. However, it is evident that the model fails to reproduce behavioral simulations of in-stream processes for most of the time.

[38] Figure 6 shows representative DO simulations of selected 24 h periods at both study reaches during both winter and summer. The behavioral models simulate the diurnal oxygen curves reasonably well, at least between the specified uncertainty bounds suggesting the main in-stream metabolic processes are broadly captured, as also implied by the successful simulation of the main differences observed between the two reaches. The same scales (per season) used in Figure 6 directly indicate this, with the observed and simulated summer and winter periods revealing larger diurnal oxygen amplitudes at the moorland site ($\sim 1.1 \text{ mg l}^{-1}$ for summer and $\sim 0.7 \text{ mg l}^{-1}$ for winter) in contrast to the forest site ($\sim 0.7 \text{ mg l}^{-1}$ for summer and

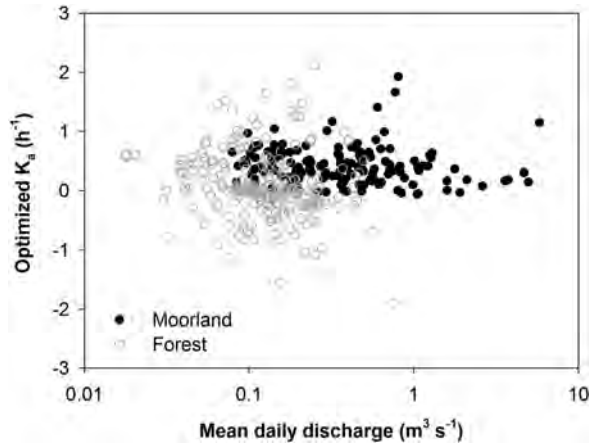


Figure 7. Optimized reaeration coefficients k_a from all accepted simulations for the moorland and forest study reaches are plotted against corresponding mean daily discharges (log-scale), respectively. Note the negative reaeration coefficients almost exclusively occur at the forest site in response to frequently observed winter oxygen supersaturation. Despite the super-saturation observed diurnal oxygen dynamics in relation to calibrated negative k_a values imply biological activity.

$\sim 0.5 \text{ mg l}^{-1}$ for winter). Also note the super-saturation of oxygen at the forest site for the winter period. This was adequately captured by the model and is not evident at the moorland site. In addition, the summer example shows a successfully simulated but unusual DO peak at 8 am in the morning. This coincides with an incoming radiation peak following a ~ 4 am sunrise and subsequent cloud cover precluding an expected DO peak at around mid-day. For the accepted simulations, the k_a parameter varied between 0.01 and 0.9 h^{-1} (90% percentiles) at the moorland site and exhibited no relationship with flow (Figure 7). However, for the forest sites a value < 0 was sometimes needed to simulate ecosystem processes under supersaturated conditions, most notably in winter.

4.3. Temporal Variability of Metabolism Dynamics and Differences Between Reaches

[39] We analyzed temporal variations in parameters using RSA as a further mean to evaluate the ability of the model to capture in-stream metabolic processes. The behavioral model parameter sets were only considered representative if they could show a distinct seasonal signal as well as capturing the diurnal oxygen cycle. Figure 8 shows cumulative efficiency plots for the five calibrated model parameters separated according to season (autumn/winter from October to March and spring/summer from April to September) and stream reach (moorland and forest). Regions of parameter identifiability (indicated by curvature) and/or constrained parameter ranges indicate seasonality and differences between sites. The reaeration parameter k_a , the photo-respiration parameter β , and the linear photosynthetic oxygen production parameter p_1 show a clear seasonal pattern at both sites. The relatively insensitive light-saturation (nonlinear) production parameter p_2 does not exhibit seasonal behavior and is similar at each site. The respiration parameter R_{20} only showed a

seasonal effect at the moorland site, but in terms of parameter range the forest site is much more constrained compared to the moorland reach. This is also visible from Table 2 indicating the 10th and 90th percentiles of behavioral (accepted) model simulations. Note that selected photo-respiration parameters (β) converge toward zero specifically over the summer period and thus effectively reduced the model structure to four parameters. This potentially indicates that during summer photo-respiration is less significant due to the higher energy potential for metabolic processes caused by high in-stream temperatures.

[40] Figure 9 shows mean monthly plots of modeled daily in-stream processes in terms of the production-respiration ratio (P/R) and the difference between production and respiration as a proxy for net ecosystem productivity (NEPc). Note that c represents the conversion of oxygen units into carbon units using the stoichiometric ratio $C/O = 0.375$ as a conversion factor assuming a respiratory quotient of 1 similar to *Gazeau et al.* [2004]. Generally, the simulations indicate a heterotrophic system ($P/R < 1$) and a potential source of carbon to the atmosphere at both sites. This is due to ER exceeding GPP most of the time with a daily range of -0.15 to $-49.8 \text{ g O}_2 \text{ m}^{-2} \text{ d}^{-1}$ (ER) and 0.15 to $23.6 \text{ g O}_2 \text{ m}^{-2} \text{ d}^{-1}$ (GPP) at the moorland reach and -0.07 to $-54.4 \text{ g O}_2 \text{ m}^{-2} \text{ d}^{-1}$ (ER) and 0.07 – $51.7 \text{ g O}_2 \text{ m}^{-2} \text{ d}^{-1}$ (GPP) at the forest reach over the study period,

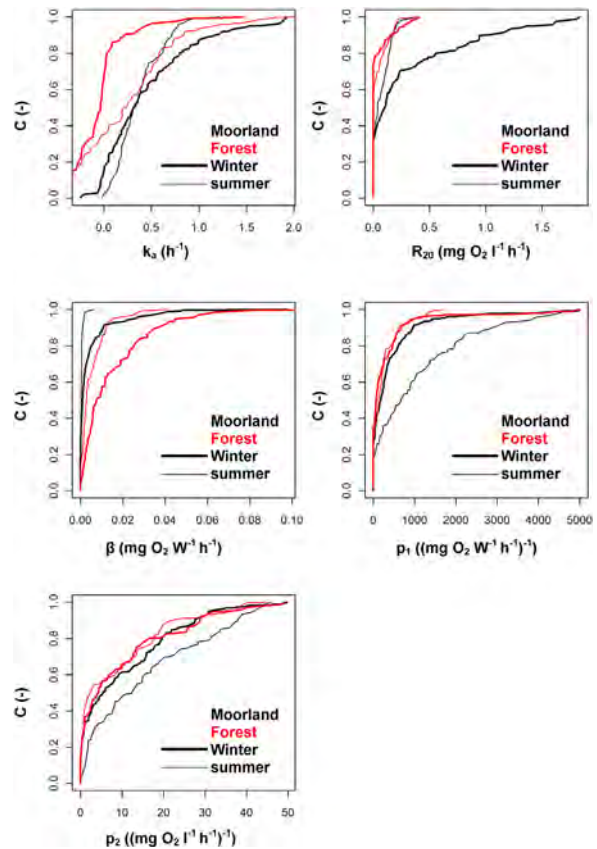


Figure 8. Regional sensitivity analysis of model parameters for both the moorland (black lines) and forest (red lines) study reaches generated from accepted simulations for summer (1 April to 30 September, thin lines) and winter (1 October to 31 March, thick lines) periods.

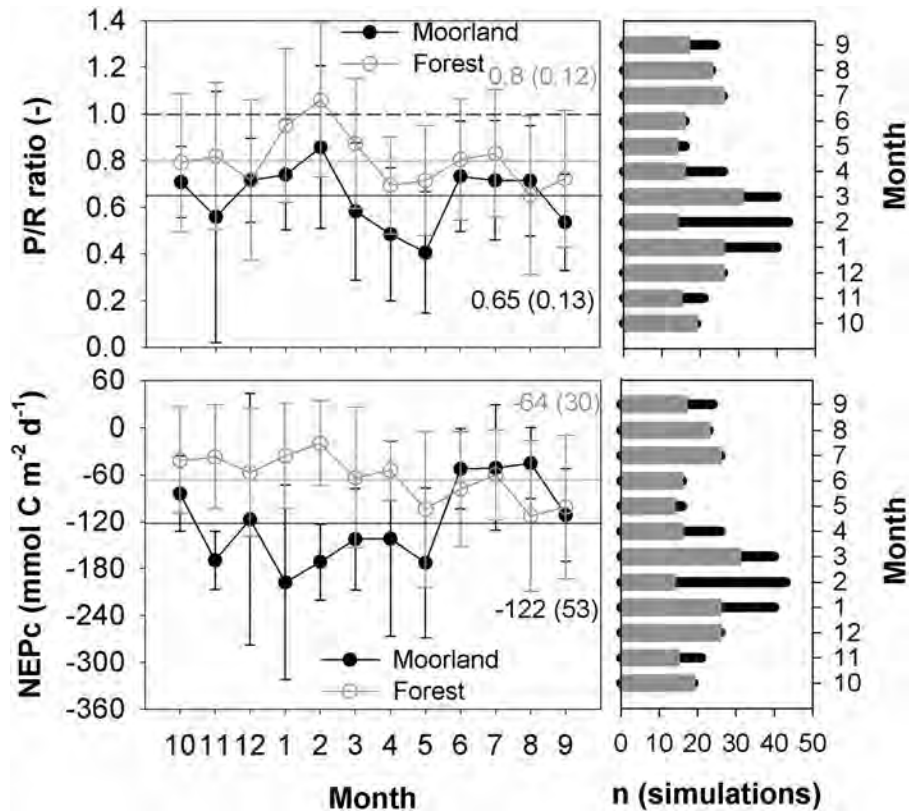


Figure 9. Mean monthly P/R ratios and net ecosystem production ($NEPc = Pc - Rc$ – converted into Carbon units) for both sites are shown. Mean values and standard deviations in parentheses are also given. The error bars reflect the standard deviations of mean monthly P/R and NEPc derived from all behavioral models per month and the horizontal bars show the number of behavioral models per month for both sites (black-moorland and gray-forest). Note that the order of months is according to the UK hydrological year from October to September.

respectively. Mean ER and GPP estimates are generally higher at the moorland site, whereas the forest reach shows a larger range in terms of extreme values. The P/R ratio follows a similar monthly pattern at both sites, but higher values are evident at the forest reach (mean P/R = 0.8) compared to the moorland (mean P/R = 0.65). Maximum values occurred in February corresponding to the earliest warmer temperatures of the year and increased radiation inputs. For the forest site, this also precedes the leafing of riparian broadleaved trees and the consequent shading effects, where on this occasion P/R exceeded 1. The P/R ratio decreases following the February peak until May, thereafter increases again—though remaining <1 —reaching a second peak over the summer months at both sites. From Figure 9, it is evident that for the winter period a higher number of simulations are taken into account for the monthly plots at the moorland site, while for the summer similar numbers of behavioral simulations from both sites were included.

[41] Monthly NEPc dynamics differ for both study reaches with the forest site exhibiting greater carbon losses during summer and the moorland reach during winter and spring. Losses are notably reduced from the moorland stream between June and August, which are generally the period of lowest flows and highest incoming radiation. During this period, the greatest biomass growth within the

channel was observed. In contrast, the NEPc dynamics at the forest reach closely resemble those of the P/R ratios. Overall, the simulations infer that the moorland reach potentially releases double the amount of carbon to the atmosphere ($122 \text{ mmol C m}^{-2} \text{ d}^{-1}$) compared to the forest reach ($64 \text{ mmol C m}^{-2} \text{ d}^{-1}$).

4.4. Factors Influencing Simulated Metabolism Dynamics

[42] Although the model could only produce acceptable simulations for about 40 and 32% of the total study period at the moorland and forest site, respectively, it was conspicuous that the rejected models generally coincided with periods where streamflows exceeded the mean flow of the Girnock. For all behavioral models, 66% were below the mean discharge of $0.62 \text{ m}^3 \text{ s}^{-1}$ at the forest reach and 56% were below the mean discharge of $0.57 \text{ m}^3 \text{ s}^{-1}$ at the moorland reach. This implies that the hydrology of the Girnock has an important effect on stream metabolism that is not captured by simpler oxygen models. This probably reflects the greater depths of more DOC-rich water at high flows which impede and disturb metabolic processes in a way that is uncertain, seasonal, and may include scour which affects the biomass of primary producers. However, Figure 5 also shows behavioral models for a range of low and high flows at both stream reaches. Interestingly,

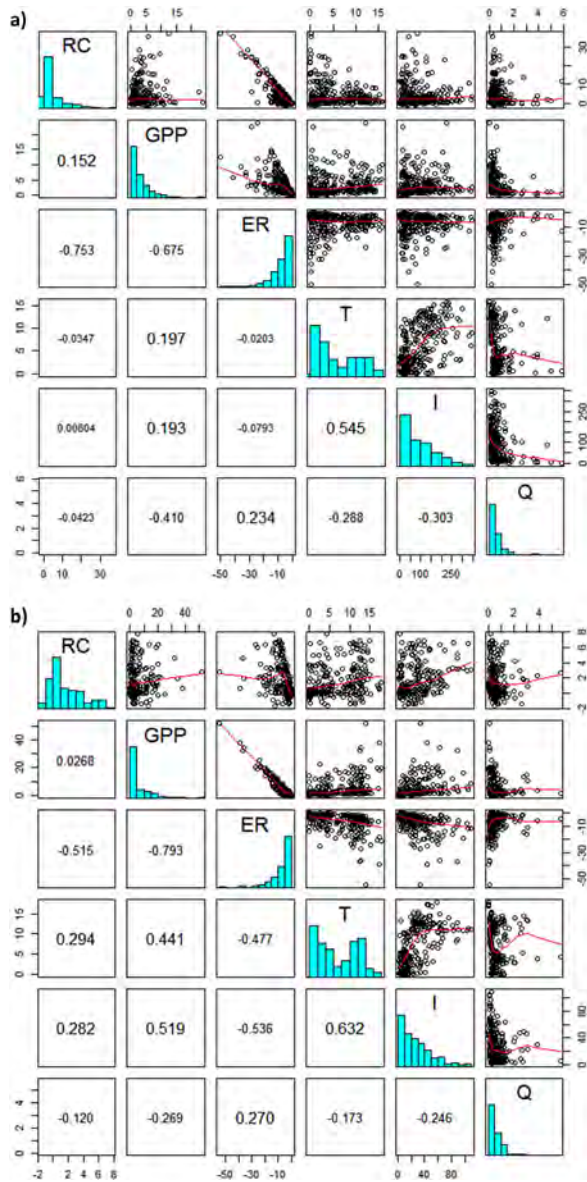


Figure 10. Bivariate plots of simulated daily stream metabolism (RC, GPP, and ER) from accepted models at (a) the moorland and (b) the forest site showing histograms and smooth curves indicating potential linear and/or non-linear relationships with environmental variables (mean daily stream temperature T, radiation I, and discharge Q). Spearman correlation coefficients are given in the lower plots, respectively.

behavioral models exceeding mean flow conditions were found almost exclusively during recession of high flow events (not easily visible from Figure 5). In addition to the obvious difference in riparian vegetation between the moorland and forest reaches (Table 1), we also assessed potential cause-effect relationships of environmental variables on behavioral simulations and derived stream metabolism (Figure 10). Reaeration did not show any significant relationship with streamflow for both sites, which is shown in the bivariate plots in Figure 10. However, estimated reaeration fluxes (shown by k_a) significantly differ between the reaches with the forest reach generally exhibiting nega-

tive values during the winter (Table 2, Figure 7). This might be related to the frequently observed supersaturation during this period (Figure 5) most likely caused by the 2 m high weir located about 300 m upstream from the forest measurement site. Furthermore, GPP estimates are only negatively correlated ($p < 0.01$) with streamflow at the moorland reach, which implies that hydrological disturbance to photosynthesis is greater in the moorland reach compared to the forest reach which is in any case characterized by lower radiation input resulting in lower photosynthesis rates regardless of flows. This might also be related to higher carbon losses during winter at the moorland site when flows normally are higher compared to summer.

[43] Only the forest reach showed significant relationships between GPP (positive) and ER (negative) with temperature and radiation. The expected positive relationship between radiation and temperature with GPP ($r = 0.2$ and $r = 0.24$, respectively) was also detected for the moorland reach, but was not statistically significant. This gives some confidence in the model calibration procedure in terms of accepting and rejecting behavioral models reflecting the physical response of in-stream metabolism to radiation and temperature (photosynthesis and oxygen production generally increase with radiation and temperature, see also Figure 4). The correlations in Figure 10 show a tight negative coupling between producers as indicated by GPP and consumers as reflected in ER ($r = -0.68$ and $r = -0.79$) and between RC and ER ($r = -0.75$ and $r = -0.51$) at the moorland and forest reaches, respectively.

5. Discussion

5.1. How Well Do Simple Oxygen Mass Balance Models Capture Metabolism in Upland Streams?

[44] Oxygen mass balance models have a long tradition in aquatic science as an alternative to incubation methods, which directly measure community production and respiration, but are more difficult to upscale [Staeher *et al.*, 2012]. However, most applications in lotic systems focus on higher-order lowland streams, which generally exhibit larger productivity, resulting in more marked (larger amplitude) diurnal DO signals compared to lower-order upland streams [Cox, 2003]. Preliminary tests have shown that the night-time regression method by Kelly *et al.* [1974] is not suitable to be applied to upland streams such as the Gironck as DO changes are frequently below 1 mg l^{-1} . As our results show, the flashy hydrodynamics play an important role in the Gironck (a third-order stream) as they can disturb diurnal DO cycles masking in-stream metabolism in a way that oxygen models such as the one used cannot account for [Demars *et al.*, 2011a]. This is due to increases in water depth at high flows, and concomitant decreases in water clarity (from DOC and turbidity), reducing radiation inputs to the stream bed, as well as potentially scouring benthic vegetation. Furthermore, other processes may also be important, but are not captured. For example, it has been recognized that streambed biofilms comprised of algae and bacteria retain nutrients independent of the stream water nutrient supply [e.g., Battin, 2000]. It also remains a major uncertainty as to how much biological activity in the hyporheic zone contributes to the whole stream metabolism [Marmonier *et al.*, 2012]. These processes could potentially

be incorporated into oxygen models, but in the absence of suitable data at the likely expense of increased parameterization. Nevertheless, this issue is the subject of future work.

[45] The advent of robust and stable optical sensors able to generate high-resolution DO data over longer time periods (>1 year) allows assessment of production and respiration processes at temporal scales from hours to years [see *Roberts et al.*, 2007]. Such data compensate for the relatively high rejection rate of model simulations in terms of identifying periods when the diurnal DO signal is clear enough for the oxygen mass balance model to account for system function [*Ciavatta et al.*, 2008]. Selection of behavioral simulations requires a flexible modeling approach using a set of governing equations that can be allowed to vary during the calibration procedure. Here, the class of evolution optimization algorithms provides a useful tool that is able to learn and improve generations of model parameter populations [*Price et al.*, 2006]. Furthermore, a rigorous posterior analysis—rejecting any simulations that do not meet required acceptable thresholds—of one or more performance criteria enables a more thorough assessment of other in-stream processes that may affect metabolism. Generally, when flows are below the mean, the behavioral simulations fit the observed DO dynamics reasonably well (Figure 5) and resulted in better performance (SSE) compared to behavioral models above mean flows. The results indicated some expected characteristics of system function, showing clear seasonality with increased production during summer and heterotrophic systems at both sites. Previous work by *Dawson et al.* [2009] had used a regional study of streamwater EpCO₂ to show that the Gironck and similar upland streams in the Scottish Highlands are heterotrophic systems throughout the year. The P/R ratios estimated in this study are similar to those reported from headwater streams in Iceland (average P/R ~ 0.6) with varying stream temperature over a summer field season [*Demars et al.*, 2011a] and higher than those (annual P/R between 0.3 and 0.4) shown by *Robert et al.* [2007] from the less productive first-order Walker Branch experimental forest stream, USA. The estimated daily GPP and ER ranges (see section 4.4) fall in between global values from *Battin et al.* [2008] and the values presented by *Demars et al.* [2011a]. Interestingly, the maximum P/R ratios were estimated for February at both reaches, which also coincides with increasing radiation inputs and stream temperatures, open canopy conditions in the forest and in-stream vegetation (macrophytes and algae) growth was frequently observed in the study reaches during that period. This also coincides with increases in other important biological activity in the Gironck, such as invertebrate drift and salmon growth [*Bacon et al.*, 2005].

[46] There is a need to further evaluate concurrent photosynthesis, respiration, and re-aeration simulations avoiding potentially misleading results [*Valino et al.*, 2005]. Specifically, the calibration of the reaeration parameter k_a introduces considerable uncertainty, but without repeated and expensive tracer-gas measurements no viable alternative is available. Even novel sound pressure-reaeration relationships require tracer-gas evasion measurements for calibration [*Morse et al.*, 2007]. The sensitivity analysis of accepted parameter sets generally showed a colinearity

index below a critical threshold ($\gamma = 20$) indicating practical identifiability [*Soetaert and Petzold*, 2010]. However, any process that would be incorporated into the existing model at the expense of increased parameterization is also likely to increase colinearity and nonuniqueness of solutions. Therefore, the five-parameter model presented is probably the highest parameterization possible while retaining identifiability (Figure 5). Nevertheless, the parameter sensitivity analysis gives some confidence that this type of flexible process model might be transferable to other well-aerated systems as an alternative to applying empirical hydraulic relationships where no reaeration measurements exist. This is similar to *Holtgrieve et al.* [2010] who successfully developed a Bayesian approach for oxygen mass balance modeling with explicit calibration of reaeration as a model parameter. Furthermore, no k_a -discharge relationship was found (Figure 7) from the behavioral simulations indicating little hydrodynamic influence on air-water oxygen exchange. Although this may seem surprising and counterintuitive, it is consistent with the findings of *Genereux and Hemond* [1992], though contrasts with the inference of empirical hydraulic relationships [see *Aristegi et al.*, 2009]. It can also be argued that negative k_a coefficients are nonphysical, but the calibration procedure effectively filtered out the winter oxygen super-saturation events showing diurnal oxygen patterns similar to Figure 6b. These events almost exclusively occur at the Forest site implying some biological activity. However, the model could only reproduce diurnal oxygen patterns under super-saturated conditions allowing for an oxygen flux from the atmosphere to the water. It is, however, reassuring that only positive values for k_a are calibrated for the moorland site. The most likely reason for these results is that in the Gironck, the channel morphology has a high degree of hydraulic roughness throughout the system (see Figure 1) due to the boulder-dominated nature of the stream [*Moir et al.*, 2004] thus ensuring high levels of reaeration at all flows. This is further pronounced at the forest site, by the weir structure at the fish trap which provides a 2 m hydraulic jump and contributes to super-saturation. The latter feature and channel characteristics of the Gironck Burn also hamper application of energy dissipation methods such as presented by *Tsivoglou and Neal* [1976].

5.2. What Do Oxygen Mass Balance Models Tell Us About the Effect of Riparian Vegetation on Stream Metabolism Dynamics?

[47] The importance of the riparian zone to the structure and function of aquatic ecosystems has become apparent and a major research foci over the past two decades [e.g., *Tockner et al.*, 2002; *Naiman et al.*, 2005; *Strayer and Findlay*, 2010]. The riparian zone has also been identified as a part of the landscape where management efforts can be focused to maximize benefits to streams [e.g., *Imholt et al.*, 2012]. For example, with Scotland, the Scottish Government has ambitious plans to increase national forest cover from 9 to 25% [*Scottish Government*, 2009]. Within this overall strategy, there is particular support for riparian planting as tree cover provides shading, increases food sources to fish, and decreases peak summer water temperatures which can be beneficial to salmonids [*Malcolm et al.*, 2008]. Climate change brings added impetus to riparian

planting as a means of mitigating the effects of rising water temperatures and ecosystem change [Hrachowitz *et al.*, 2010]. However, such endeavours usually produce feedbacks and unintended consequences, including potential changes to ecosystem productivity. One goal of this work was to explore the effect of riparian vegetation on stream metabolism via a paired-reach approach with available long-term data. The most prominent effect of riparian vegetation is readily observable from Figure 2 and Table 1 in terms of substantially lower levels of incoming short-wave radiation reaching the stream. The overall mean incoming short-wave radiation at the forest site was measured at only 25.7 W m^{-2} compared to 111 W m^{-2} at the open moorland reach, despite identical variability in terms of the coefficient of variation (Table 1). This favored a stronger seasonal dependence of GPP on incoming radiation at the forest reach ($r=0.52$) compared to the observed but smaller seasonality effect at the more light abundant moorland reach ($r=0.24$, Figure 10). However, GPP rates were greater at the open moorland site during summer most likely due to a larger biomass as shown by Young and Huryn [1999]. Interestingly, GPP exhibited an almost negative linear relationship with ER at the forest site, whereas such a relationship is weaker and more variable at the moorland site (Figure 10). Differences in the GPP-ER relationship may be explained by variability in nutrient cycling similar to Demars *et al.* [2011a]. Organic nitrogen and phosphorous probably increase in the forest in spring and autumn when allochthonous inputs from the trees increase compared to the in general low nutrient status at the moorland site. Overall, our results point to the forest site being a smaller carbon source to the atmosphere compared to the moorland reach, where particularly during winter, greater respiration rates appear to cause more carbon to be released. However, these results have to be viewed with caution. The daily NEP based on the difference between GPP and ER estimates can only be viewed as a proxy for whole stream ecosystem metabolism and is strictly only valid under steady state conditions [Gazeau *et al.* 2004]. Furthermore, uncertainties around GPP and ER estimates are high and it is likely that the thermal regimes at both reaches are not only affected by distinct incoming radiation patterns, but also by distinct hyporheic characteristics. For example, a much larger hyporheic volume and exchange can be assumed at the forest reach compared to the moorland site due to the more alluvial nature of the downstream reach [Malcolm *et al.*, 2008]. Hyporheic water exchange has been shown to be an important factor controlling ER [Mulholland *et al.*, 2001]. Moreover, Demars *et al.* [2011b] reported that water transient storage of the hyporheic zone controls ER with a greater hyporheic volume most likely increasing ER. Furthermore, differences between the reaches and in-stream metabolic processes can be caused by the nonlinear response of P and R to temperature. Demars *et al.* [2011a] showed greater temperature dependence of ER compared to GPP. This type of effect is consistent with our findings of greater ER at the moorland reach.

6. Conclusions

[48] In this study, we presented a relatively simple oxygen mass balance model calibrated to high-resolution and

long-term DO data from two distinct stream reaches in the upland Girnock Burn in Scotland. The model comprised a maximum of five parameters representing processes of dark and light community respiration, linear and light-saturation photosynthetic productivity, and air-water gas exchange. These parameters were successively fitted to 24 h periods deriving a unique set of time-variable parameters for the moorland and forest study reaches. Only simulations that fulfilled criteria evaluating the form of simulated diurnal oxygen curves around the mean concentration with respect to observed values were accepted for further analysis. Sensitivity analysis showed that 95% of the accepted parameter sets were uniquely identifiable. This suggests that the flexible model framework in combination with an efficient calibration and posterior analysis may be transferable to other systems. Also, simultaneous calibration of P, R, and reaeration is viable in places with available long-term oxygen data, but where no reaeration measurements exist and where the air-water gas exchange does not show a significant hydraulic relationship with e.g., discharge. Based on the retained simulations, we could show a typical seasonal behavior (winter/summer) of stream metabolism and differences between the moorland and the forest stream reaches which appear to be disrupted by the flashy hydrodynamics of the system. Although preliminary, our results indicate that riparian afforestation could decrease carbon release to the atmosphere through decreased stream metabolism. However, to further underpin such results and inform policy makers, future research on nutrient cycling, hyporheic biological activity, hyporheic exchange and groundwater-surface water interactions, and their role on stream metabolism dynamics at the catchment scale is required. Although there is a clear need to assess how stream metabolism dynamics might behave in the future due to environmental change, the presented modeling framework represents a first step in this direction.

Notation

| | |
|--------------------|---|
| DO | Dissolved oxygen [mg l^{-1}] |
| R | Community respiration [$\text{mg O}_2 \text{l}^{-1} \text{h}^{-1}$] |
| P | Community photosynthetic production [$\text{mg O}_2 \text{l}^{-1} \text{h}^{-1}$] |
| RC | Re-aeration capacity [$\text{mg O}_2 \text{l}^{-1} \text{h}^{-1}$] |
| GPP | Global photosynthetic production [$\text{mg O}_2 \text{l}^{-1} \text{d}^{-1}$] |
| ER | Ecosystem respiration [$\text{mg O}_2 \text{l}^{-1} \text{d}^{-1}$] |
| t | time |
| v | Mean stream velocity [m s^{-1}] |
| Q | Discharge [$\text{m}^3 \text{s}^{-1}$] |
| h | Stream depth [m] |
| w | Stream width [m] |
| P_E | Altitudinally corrected air pressure [kPa] |
| V | Saturation water vapor pressure [kPa] |
| O_s | Expected oxygen solubility [mg l^{-1}] |
| O_s^{atm} | Oxygen solubility under normal pressure [mg l^{-1}] |
| P_{msl} | Pressure at mean sea level [kPa] |
| E | Elevation of observed pressure [m] |
| AT | Air temperature [K] |
| g | $9.806 \text{ [m s}^{-2}\text{]}$ |
| m | Molecular mass of dry air [kg mol^{-1}] |
| k | Boltzmann constant [J K^{-1}] |
| T | Stream temperature [$^{\circ}\text{C}$] |
| θ | Arrhenius coefficient [-] |

| | |
|--------------------------|--|
| k_a | Re-aeration coefficient [h^{-1}] |
| I | Incoming short-wave radiation [W m^{-2}] |
| R_{20} | Respiration rate parameter [$\text{mg O}_2 \text{ l}^{-1} \text{ h}^{-1}$] |
| β | Photorespiration parameter [$\text{mg O}_2 \text{ W}^{-1} \text{ h}^{-1}$] |
| p_1 | Linear photosynthesis parameter [$(\text{mg O}_2 \text{ W}^{-1} \text{ h}^{-1})^{-1}$] |
| p_2 | Light saturation parameter [$(\text{mg O}_2 \text{ l}^{-1} \text{ h}^{-1})^{-1}$] |
| n | Number of 24-h periods |
| j | Time step [hourly] |
| DO_{sim} | Predicted DO |
| DO_{obs} | Observed DO |
| SSE | Sum of squared errors objective function [mg l^{-1}] |

[49] **Acknowledgments.** We would like to thank SEPA for discharge and manual flow gauging data, BADC for access to climate data, FRS staff for field and laboratory work, Richard Smart for sampling water quality data, and Mike Kennedy for the plant survey and species identification. Constructive comments from the Editor, Associate Editor, and anonymous reviewers are greatly acknowledged.

References

- Andrews, F., B. Croke, and A. Jakeman (2011), An open software environment for hydrological model assessment and development, *Environ. Modell. Software*, 26, 1171–1185, doi:10.1016/j.envsoft.2011.04.006.
- Aristegi, L., O. Izagirre, and A. Elosegi (2009), Comparison of several methods to calculate reaeration in streams, and their effects on estimation of metabolism, *Hydrobiologia*, 635, 113–124, doi:10.1007/s10750-009-9904-8.
- Aufdenkampe, A. K., E. Mayorga, P. A. Raymond, J. M. Melack, S. C. Doney, S. R. Alin, R. E. Aalto, and K. Yoo (2011), Riverine coupling of biogeochemical cycles between land, oceans, and atmosphere, *Frontiers Ecol. Environ.*, 9(1), 53–60, doi:10.1890/100014.
- Bacon, P. J., W. S. C. Gurney, W. Jones, I. S. McLaren, and A. F. Youngson (2005), Seasonal growth patterns of wild juvenile fish: Partitioning variation among explanatory variables, based on individual growth trajectories of Atlantic salmon (*Salmo salar*) parr, *J. Animal Ecol.*, 74, 1–11, doi:10.1111/j.1365-2656.2004.00875.x.
- Battin, T. J. (2000), Hydrodynamics is a major determinant of streambed biofilm activity: From the sediment to the reach scale, *Limnol. Oceanogr.*, 45, 1308–1319.
- Battin, T. J., L. A. Kaplan, S. Findlay, C. S. Hopkinson, E. Marti, and A. I. Packman, J. D. Newbold, and F. Sabater (2008), Biophysical controls on organic carbon fluxes in fluvial networks, *Nat. Geosci.*, 1, 95–100.
- Beven, K. (2012), *Rainfall-Runoff Modelling: The Primer*, 2nd ed., Wiley-Blackwell, Chichester, U. K.
- Birkel, C., D. Tetzlaff, S. M. Dunn, and C. Soulsby (2010), Towards simple dynamic process conceptualization in rainfall-runoff models using multi-criteria calibration and tracers in temperate, upland catchments, *Hydrol. Processes*, 24, 260–275.
- Birkel, C., D. Tetzlaff, S. M. Dunn, and C. Soulsby (2011), Using time domain and geographic source tracers to conceptualize streamflow generation processes in lumped rainfall-runoff models, *Water Resour. Res.*, 47, W02515, doi:10.1029/2010WR009547.
- Bott, T. (2006), Primary productivity and community respiration, in *Methods in Stream Ecology*, edited by F. R. Hauer, and G.A. Lamberti, Academic, Amsterdam.
- Brun, R., P. Reichert, and H. Kunsch (2001), Practical identifiability analysis of large environmental simulation models, *Water Resour. Res.*, 37(4), 1015–1030.
- Ciavatta, S., R. Pastres, C. Badetti, G. Ferrari, and M. B. Beck (2008), Estimation of phytoplanktonic production and system respiration from data collected by a real-time monitoring network in the Lagoon of Venice, *Ecol. Modell.*, 212(1-2), 28–36, doi:10.1016/j.ecolmodel.2007.10.025.
- Cole, J. J., Y. T. Prairie, N. F. Caraco, W. H. McDowell, L. J. Tranvik, and R. G. Striegl (2007), Plumbing the global carbon cycle: Integrating inland waters into the terrestrial carbon budget, *Ecosystems*, 10, 171–184.
- Cox, B. (2003), A review of dissolved oxygen modelling techniques for lowland rivers, *Sci. Total Environ.*, 314–316, 303–334.
- Dawson, J. J. C., C. Soulsby, M. Hrachowitz, M. Speed, and D. Tetzlaff (2009), Seasonality of epCO₂ in an integrated river continuum, *Hydrol. Processes*, 23, 2929–2942, doi:10.1002/hyp.7402.
- Demars, B. O. L., J. R. Manson, J. Ólafsson, J. S. Gíslason, G. M. Gudmundsdóttir, R. Woodward, G. Reiss, D. E. Pichler, J. J. Rasmussen, and N. Friberg (2011a), Temperature and the metabolic balance of streams, *Freshwater Biol.*, 56, 1106–1121, doi:10.1111/j.1365-2427.2010.02554.x.
- Demars, B. O. L., J. R. Manson, J. S. Ólafsson, G. M. Gíslason, and N. Friberg (2011b), Stream hydraulics and temperature determine the metabolism of geothermal Icelandic streams, *Knowl. Manage. Aquat. Ecosyst.*, 402(5), doi:10.1051/kmae/2011046.
- Elmore, H. L. and W. F. West (1961), Effect of water temperature on stream reaeration, *J. Sanit. Eng. Div.*, 87, 59–71.
- Geneux, D. P. and H. F. Hemond (1992), Determination of gas exchange rate constants for a small stream on walker branch watershed, Tennessee, *Water Resour. Res.*, 28(9), 2365–2374.
- Gazeau, F., S. V. Smith, B. Gentili, M. Frankignoulle, and J. P. Gattuso (2004), The European coastal zone: Characterization and first assessment of ecosystem metabolism, *Estuarine Coastal Shelf Sci.*, 60, 673–694.
- Hannah, D. M., I. A. Malcolm, C. Soulsby, and A. F. Youngson (2008), A comparison of forest and moorland stream microclimate, heat exchanges and thermal dynamics, *Hydrol. Processes*, 22, 919–940.
- Hanson, P. C., S. R. Carpenter, N. Kimura, C. Wu, S. P. Cornelius, and T. K. Kratz (2008), Evaluation of metabolism models for free-water dissolved oxygen methods in lakes, *Limnol. Oceanogr.*, 6, 454–465.
- Holtgrieve, G. W., D. E. Schindler, T. A. Branch, and Z. T. A'mar (2010), Simultaneous quantification of aquatic ecosystem metabolism and reaeration using a Bayesian statistical model of oxygen dynamics, *Limnol. Oceanogr.*, 55(3), 1047–1063.
- Hornberger, G., and R. Spear (1981), An approach to the preliminary analysis of environmental systems, *J. Environ. Manage.*, 12, 7–18.
- Hrachowitz, M., C. Soulsby, C. Imholt, I. A. Malcolm, and D. Tetzlaff (2010), Thermal regimes in a large upland salmon river: A simple model to identify the influence of landscape controls and climate change on maximum temperatures, *Hydrol. Processes*, 24(23), 3374–3391.
- Imholt, C., C. Soulsby, I. A. Malcolm, M. Hrachowitz, C. N. Gibbins, S. Langan, and D. Tetzlaff (2012), Influence of scale on thermal characteristics in a large Montane river basin, *River Res. Applic.*, 29, 403–419, doi:10.1002/rra.1608.
- Izagirre, O., M. Bermejo, J. Pozo, and A. Elosegi (2007), RIVERMET©: An Excel-based tool to calculate river metabolism from diel oxygen-concentration curves, *Environ. Modell. Software*, 22(1), 24–32, doi:10.1016/j.envsoft.2005.10.001.
- Kelly, M. G., G. M. Hornberger, and B. J. Cosby (1974), Continuous automated measurement of rates of photosynthesis and respiration in an undisturbed river community, *Limnol. Oceanogr.*, 19, 305–312.
- Malcolm, I. A., A. F. Youngson, and C. Soulsby (2005), Hydrological processes in the hyporheic zone determine salmonid embryo survival and performance, *J. Fish Biol.*, 67, 270–271.
- Malcolm, I. A., C. Soulsby, and A. F. Youngson (2006), High frequency logging technologies reveal state dependence of hyporheic process dynamics: Implications for hydroecology, *Hydrol. Processes*, 20, 615–622.
- Malcolm, I. A., C. Soulsby, D. M. Hannah, P. J. Bacon, A. F. Youngson, and D. Tetzlaff (2008), The influence of riparian woodland on stream temperatures: Implications for the performance of juvenile salmonid, *Hydrol. Processes*, 22, 968–979.
- Malcolm, I. A., A. F. Youngson, C. Soulsby, C. Imholt, and R. J. Fryer (2011), Is interstitial velocity a good predictor of salmonid embryo survival?, *Trans. Am. Fish. Soc.*, 140(4), doi:10.1080/00028487.2011.601216.
- Marmonier, P., G., et al. (2012), The role of organisms in hyporheic processes: Gaps in current knowledge, needs for future research and applications, *Annal. Limnol.—Int. J. Limnol.*, 48, 253–266, doi:10.1051/limn/2012009.
- Moir, H., C. Soulsby, and A. F. Youngson (2002), The hydraulic and sedimentary controls on the availability of Atlantic salmon spawning habitat in the river system NE Scotland, *Geomorphology*, 45, 291–308.
- Moir, H., C. N. Gibbins, C. Soulsby, and J. Webb (2004), Linking channel geomorphic characteristics to spatial patterns of spawning activity and discharge use by Atlantic salmon (*Salmo salar* L.) in two upland Scottish streams, *Geomorphology*, 60(1-2), 21–35.
- Morse, N., W. B. Bowden, A. Hackman, C. Pruden, E. Steiner, and E. Berger (2007), Using sound pressure to estimate reaeration in streams, *J. North Am. Benthol. Soc.*, 26, 28–37.
- Mulholland, P. J., et al. (2001), Inter-biome comparison of factors controlling stream metabolism, *Freshwater Biol.*, 46, 1503–1517.

- Mullen, K., D. Ardia, D. Gil, D. Windover, and J. Cline (2011), DEoptim: An R package for global optimization by differential evolution, *J. Stat. Software*, 40(6), 1–26.
- Naiman, R. J., N. Décamps, and M. E. McClain (2005), *Riparia: Ecology, Conservation, and Management of Streamside Communities*, Academic Press, San Diego, Calif.
- Odum, H. T. (1956), Primary production in flowing waters, *Limnol. Oceanogr.*, 2, 102–117.
- Parkhurst, K., and J. S. Gulliver (1998), Application of photorespiration concepts to whole stream productivity, *Hydrobiologia*, 389, 7–19.
- Price, K., R. M. Storn, and J. A. Lampinen (Eds.) (2006), *Differential Evolution: A Practical Approach to Global Optimization*, Nat. Comput. Ser., Springer, Berlin, Germany.
- R Development Core Team (2010), *R: A Language and Environment for Statistical Computing*, R Found. for Stat. Comput., Vienna.
- Roberts, B. J., P. J. Mulholland, and W. R. Hill (2007), Multiple scales of temporal variability in ecosystem metabolism rates: Results from two years of continuous monitoring in a forested headwater stream, *Ecosystems*, 10(4), 588–606.
- Scottish Government (2009), *The Scottish Government's Rationale For Woodland Expansion*, For. Comm., Edinburgh.
- Smart, R. P., C. Soulsby, M. Cresser, A. Wade, and M. F. Billett (2001), Riparian zone influence on stream water chemistry at different spatial scales: A GIS based approach, *Sci. Total Environ.*, 280, 173–193.
- Soetaert, K., and T. Petzoldt (2010), Inverse modelling, sensitivity and Monte Carlo analysis in r using package FME, *J. Stat. Software*, 33(3), 1–28.
- Staehr, P. A., J. M. Testa, W. M. Kemp, J. J. Cole, K. Sand-Jensen, and S. V. Smith (2012), The metabolism of aquatic ecosystems: History, applications, and future challenges, *Aquat. Sci.*, 74, 15–29, doi:10.1007/s00027-011-0199-2.
- Strayer, D. L. and S. E. G. Findlay (2010), Ecology of freshwater shore zones, *Aquat. Sci.*, 72, 127–163, doi:10.1007/s00027-010-0128-9.
- Tetzlaff, D., C. Soulsby, S. Waldron, I. A. Malcolm, P. J. Bacon, S. M. Dunn, and A. Lilly (2007), Conceptualisation of runoff processes using GIS and tracers in a nested mesoscale catchment, *Hydrol. Processes*, 21, 1289–1307.
- Tetzlaff, D., C. Soulsby, and C. Birkel (2010), Hydrological connectivity and microbiological fluxes between landscapes and riverscapes: The importance of seasonality, *Hydrol. Processes*, 24, 1231–1235.
- Thomson, J., J. Bryce, R. Scott, and D. Horsfield (2006), Deer management, in *The Nature of the Cairngorms—Diversity in a Changing Environment*, edited by S. Thompson, pp. 367–380, Scottish Natural Heritage, Edinburgh.
- Tockner, K., J. V. Ward, P. J. Edwards, and J. Kollmann (2002), Riverine landscapes: An introduction, *Freshw. Biol.*, 47, 497–500.
- Tsvoglou, E. C., and L. A. Neal (1976), Tracer measurement of reaeration: Predicting reaeration capacity of inland streams, *J. Water Pollut. Control Fed.*, 48, 2669–2689.
- Uehlinger, U., C. Koenig, and P. Reichert (2000), Variability of photosynthesis-irradiance curves and ecosystem respiration in a small river, *Freshwater Biol.*, 44, 493–507.
- Valino, J. J., C. S. Hopkinson, and R. H. Garrit (2005), Estimating estuarine gross production, community respiration and net ecosystem production: A nonlinear inverse technique, *Ecol. Model.*, 187, 281–296.
- Williamson, C. E., W. Dodds, T. K. Kratz, and M. A. Palmer (2008), Lakes and streams as sentinels of environmental change in terrestrial and atmospheric processes, *Front. Ecol. Environ.*, 6, 247–254.
- Young, R. G., and A. D. Huryn (1999), Effects of land use on stream metabolism and organic matter turnover, *Ecol. Appl.*, 9, 1359–1376.